Investigating the Capabilities of Popular Turbulence Models in Recreating the Flow Over a Sharp Edged Flat Plate at Incidence

Alasdair Christison Gray[*]

University of Edinburgh

The complex case of flow past a sharp edged flat plate at incidence has been modelled using K-ω and K-ω SST turbulence models both with and without a Durbin scale limiter and an anisotropic Reynolds Stress model. Whilst the Reynolds stress models produced unphysical results, the K-ω performed slightly better. The SST model, when used without a scale limiter, was able to predict the reattachment length to within 0.5% but none of the models were able to predict more subtle flow features such as the correct boundary layer development, the distribution of TKE and the relaminarisation of the reversed boundary layer leading to the formation of a secondary separation bubble.[†]

I.   Introduction

This study focuses on the accuracy of modelling the separated flow over a thin, flat plat aerofoil with a sharp leading edge at incidence with various turbulence models. The computational study is designed to recreate the experiments carried out by Crompton [1] and results are compared to those from Crompton's experimental work. The flow past thin aerofoils with sharp leading edges is particularly important to the understanding of flow past sails, and other membrane style aerofoils, something which is not yet fully understood and that presents significant challenges to traditional turbulence models. This study concentrates on evaluating the performance of the K-ω, K-ω SST and Reynolds Stress Transport models, similar studies have been conducted previously by Collie, Gerritsen and Jackson [2], Rezende and Nieckele [3] and Sampaio, Rezenda and Nieckele [4] but in domains differing from the experimental setup of Crompton.

A.   Characteristics of Flow past a Flat Plate at Incidence

Figure 1 shows the general structure of the flow over a flat, sharp leading edge plate at low incidence. The leading edge geometry causes flow over the top surface to immediately separate, forming a shear layer. The shear layer undergoes transition close to the leading edge and consequently begin to thicken at an increased rate, eventually bending back towards the plate and reattaching. At the reattachment point an unusual turbulent boundary layer is formed with an almost linear profile, moving downstream, a non traditional turbulent boundary layer profile develops with a very thin region of very steep velocity gradient followed by a much shallower, near constant velocity gradient extending to the freestream, indicating the injection of turbulence into the near wall region from above. Turbulence kinetic energy peaks in the shear layer around the midpoint of the separation bubble before being damped as flow approaches the reattachment point, this partially due to the natural decrease in turbulence towards a stagnation point and partially due to the bifurcation of the flow which breaks large eddies into smaller ones. Inside the recirculation bubble, the reversed boundary layer undergoes a relaminarisation, leaving it more susceptible to separation as it experiences the adverse pressure gradient approaching the leading edge. This separation forms a secondary recirculation bubble rotating in the opposite direction to the primary bubble [1].
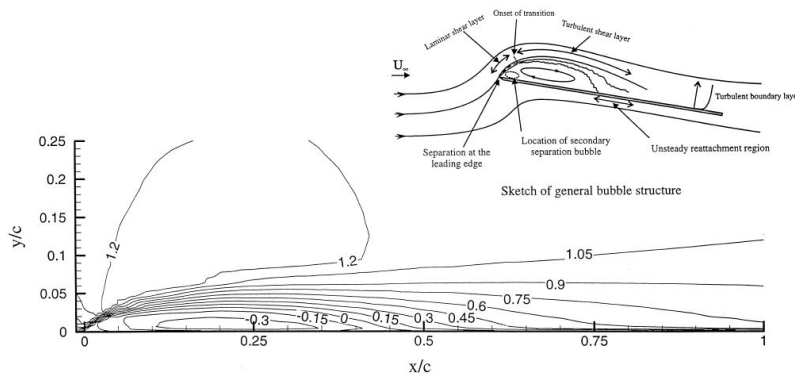

Figure 1. Normalised chordwise velocity profile for Re = $2.13 \times 10^5, \alpha = 3°$ and general structure of flat plate separation bubble [1]

These features present a number of challenges for traditional turbulence models as identified by Collie et al [2] and Sampaio et al [4]. Firstly the unsteadiness at the leading edge feeds into the downstream turbulent spectrum affecting the post reattachment boundary layer profile. Next, as the flow approaches the reattachment point, velocity fluctuations perpendicular to the plate reduce and transfer their energy to chordwise fluctuations, the majority of turbulence models, which assume that the Reynolds stresses are isotropic, cannot model this energy transfer and thus predict a reduction in the level of TKE (TKE) [2]. Finally, the turbulence

---

models are unable to accurately predict both the transition to turbulence in the shear layer or the relaminarisation of the reversed boundary layer, the former is not of great consequence as this transition typically happens very close to the leading edge but the latter results in the turbulence models not predicting the formation of the secondary separation bubble. This leads to less shear at the beginning of the shear layer and thus a lower rate of production of turbulence, affecting the prediction of the reattachment point [2].

II. Computational Model

The studies presented in this report are all performed at Re $= 2.13 \times 10^5, \alpha = 3°$ due to the availability of experimental data for this case.

A. Geometry

The computational domain was created based on the dimensions given by Crompton, the same plate dimensions were used ($0.16\,\text{m}$ chord and $6\,\text{mm}$ thickness with a $20°$ chamfer on the leading edge. The wind tunnel geometry was based on the dimensions given by Crompton ($0.8\,\text{m} \times 0.6\,\text{m} \times 1.6\,\text{m}$ (width $\times$ height $\times$ length)), based on initial simulations, the lengths of the domain up and downstream of the plate were increased to 6 and 15 chordlengths respectively to minimise the influence of the uniform inlet and outlet boundary conditions on the flow round the plate. A 2D simulation is justified in this case as Crompton explains the separation bubble exhibits a constant length and flow is essentially 2D over the central 60% of the plate, including the planes in which velocity and pressure measurements were taken. The height of the tunnel was kept at $0.6\,\text{m}$ but it should be noted that this dimension did appear to interfere with the pressure and velocity field around the plate, it is unclear whether this effect was found in Crompton's wind tunnel but it may provide a source of error for Collie, Rezende and Sampaio who attempted to model the plate in a true freestream [2, 3, 4].

B. Boundary Conditions

A uniform velocity inlet was set at the leftmost boundary with a boundary normal velocity of $20\,\text{m s}^{-1}$, turbulent intensity was set at 0.05% based on the maximum value quoted by Crompton and the turbulent length scale was defined as $0.001\,\text{m}$ taken from Collie [2] as a typical scale for low turbulence wind tunnels[2], Sampaio noted that solutions were essentialy independent of inlet turbulence conditions at high Reynolds numbers due to the comparatively large production of turbulence at the leading edge [4]. A uniform pressure outlet was specified at then end of the tunnel and slip walls were defined on the top and bottom of the domain, figure 2 shows a schematic of the domain geometry and boundary conditions.
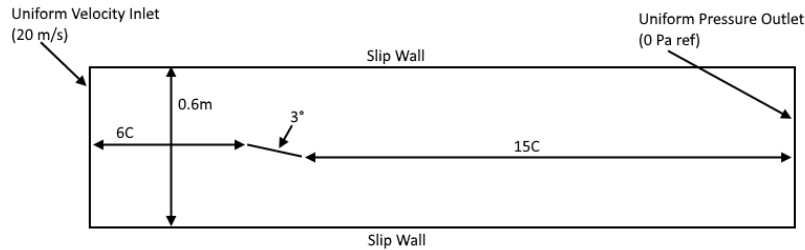

Uniform Velocity Inlet
(20 m/s)

Uniform Pressure Outlet
(0 Pa ref)

Slip Wall

0.6m

3°

6C

15C

Slip Wall

Figure 2. Computational domain and boundary conditions

C. Mesh

The domain was meshed with polyhedral elements, these elements were chosen due their sudo-random edge orientation which should allow them to better capture the recirculation bubble which is not aligned with the plate. Polyhedral cells also have more neighbouring cells than tetra or hexahedral cells which improves the computation of gradients and the number of flow directions which the cells can accurately model making them ideal for recirculating flows [5]. A prism layer was added to the plate to accurately capture the boundary layer, the first cell size was set at 1×10^{-5}m based on Collie's findings and the maximum height of the prism layer was set at $0.125C$ based on the velocity profiles measured by Crompton. The number of layers was specified to achieve an acceptable growth ratio of 1.1, this can be calculated by rearranging the equation for the sum of a geometric series:

$$S_n = a_1 \frac{1 - r^n}{1 - r} \rightarrow n = \frac{\ln\left(1 - \frac{S_n(1-r)}{a_1}\right)}{\ln(r)} \tag{1}$$

Where S_n is the total prism layer height, a_1 is the first cell height, r is the growth ratio and n is the number of layers. The prism layers were grown until they reached an aspect ratio of 1 to avoid a large cell volume ratio at the prism layer, volume mesh interface. The layer reduction percentage was set to zero to ensure a conformal prism layer. Table 1 details the mesh parameters defined at particular surfaces and edges. Many of these sizings were based on the Star CCM+ best practices for aerofoil sections [6]. An issue was encountered at the leading edge with the prism layers retracting into a single cell (see figure 3b) however this cell was judged to not be in a critical flow area and small enough not to affect the global solution. To study the effect of mesh size, 3 grids were generated with base sizes of 0.5, 1 and 2 chordlengths, the prism layer first cell height was scaled accordingly but total prism layer was kept constant as this parameter is a function of boundary layer thickness, the number of prism layers was altered to achieve the same growth ratio of 1.1 on all grids giving 48, 55 and 63 layers respectively. Grid sizes were 50199, 73434 and 104518 cells, the solutions did not show a clear trend with decreasing cell size indicative of the asymptotic region, but results did not vary greatly between meshes (see figure3a), this could indicate that the grids are not in the asymptotic region, that the differences in grid size were not great enough to indicate any trend or that the solution is grid independent at these sizes. All results presented in the results section are taken from the fine grid solutions.
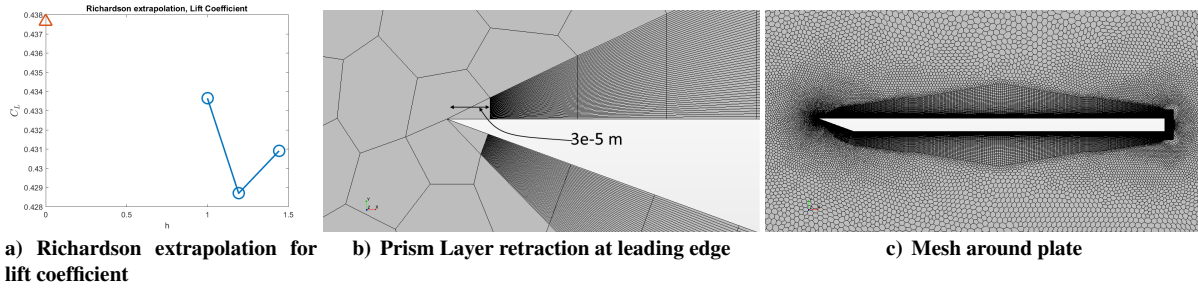
a) **Richardson extrapolation for lift coefficient**

b) **Prism Layer retraction at leading edge**

c) **Mesh around plate**

Figure 3. **Medium grid**

Table 1. **Mesh sizes**

Location	Target Surface Size	Minimum Surface Size	Surface Growth Rate
	% of base size		
Plate Surface	1	0.01	1.01
Leading Edge	0.1	0.01	-
Trailing Face	0.1	0.01	-
Outer Boundaries	100	10	1.05

D. Physics Models

Flow was modelled as steady and incompressible, incompressibility is valid given that the inlet velocity of $20\,\mathrm{m\,s}^{-1}$ represents a Mach number of approximately 0.06, the assumption of steady flow is less justified and will be discussed later. Although Star CCM+'s segregated solver is typically recommended for subsonic and incompressible flows, the coupled solver was found to give faster and more consistent convergence, it also allowed for the use of Star CCM+'s Expert Initialisation feature which initialises the flow field by solving an inviscid version of the simulation to moderate convergence on decreasingly coarse representations of the grid. The CFL number was set to 100 with a ramp starting at a value of 1 over the first 200 iterations. Simulations were run until residuals had reduced by six orders of magnitude and the lift coefficient had converged to a stable value.

Three different turbulence models were used in this study, K-ω, K-ω SST and Reynolds Stress Transport model. The K-ω SST model is generally regarded to be the most the most accurate model for the majority of applications and is capable of predicting behaviour near walls as well as in adverse pressure gradients and separating flows. The model is a variation of the standard K-ω model which behaves well near walls but tends to overpredict turbulence in the freestream, to combat this the SST version smoothly blends from K-ω in the boundary layer to K-ϵ in freestream areas, a model which predicts freestream turbulence well but cannot accurately resolve regions of high shear [7]. However it was hypothesised that this blending may leave the shear layer of the separation in the K-ϵ region which would lead to poor prediction of its behaviour, for this reason simulations were also run with the standard Wilcox K-ω model. For both K-ω and K-ω SST, simulations were run with and without the Durbin Scale Limiter, this feature essentially limits the eddy viscosity to avoid the tendency of the K-ω to predict large increases in TKE in stagnation zones [8]. It was hypothsised that the scale limiter may be reducing the generation of turbulence in the shear layer thus leading to overpredicted reattachment lengths, Collie mentions the limiter reduces the TKE values in the rear half of the bubble which leads to the underprediction of velocities on either side of the shear layer [2].To try to model the anisotropic turbulent structures near the reattachment point, simulations were also run using the Reynolds Stress Eliptical Blending turbulence model, the Eliptical Blending version of the model was chosen as it was the only available model applicable to low Y+ meshes. However, the models not only greatly overpredicted the reattachment length but also exhibit an anomolous flow behaviour, with the shear layer bending back on itself before reattching, the same anomaly was found in Rezende's Reynolds Stress simulations although they were able to accurately predict the reattachment length [3]. As such the results from these simulations will not be discussed.

III. Results

A. Separation Bubble

Figures 4a and 4b show the distributions of pressure and skin friction coefficients over the plate, the reattachment point is defined as the point at which the skin friction coefficient reaches a minimum. There is almost no difference in the pressure and skin friction distributions for the K-ω and K-ω SST models with the Durbin scale limiter with both overpredicting the reattachment length by around 35%, however turning the limiter off clearly has a large effect. In the K-ω SST simulation, removing the scale limiter has increased the turbulent production in the shear layer, moving the reattachment point back to with 0.5% of the experimental value. On the other hand the K-ω model without the Durbin limiter vastly underpredicts the reattachment length. As shown in figure 4c, this is because the model has predicted an anomolous peak in turbulence at the stagnation point of the leading edge, the level of TKE in this region is around 6 times higher than the peak value in any of the other simulation and has only been limited by the maximum value specified in the K-ω model in Star CCM+. This greatly increased level of turbulence allows the separation bubble to bend around the leading edge at a much tighter radius and thus reattach at approximately one third the experimental value. All of the models underpredict the peak suction that occurs in the recirculation region but are resonably accurate downstream of reattachment. This is because the simulations predict a flatter and larger radius separation bubble than the experiments, this increased curvature in the experimental bubble leads to greater suction. Because of it greatly increased level of turbulence, the K-ω model predicts a much tighter radius bubble and thus a much greater suction peak.
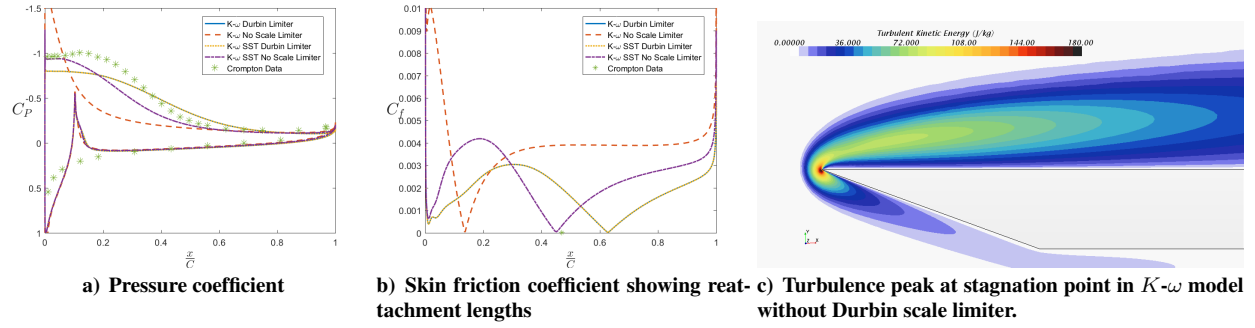
a) Pressure coefficient

b) Skin friction coefficient showing reattachment lengths

c) Turbulence peak at stagnation point in K-ω model without Durbin scale limiter.

Figure 4. Prediction of reattachment

Table 2. Comparison of reattachment length predictions

model	Experimental	K-ω with Durbin limiter	K-ω with no limiter	K-ω SST with Durbin Limiter	K-ω SST with no Limiter
$\frac{x_r}{c}$	0.47	0.656	0.159	0.624	0.468
% error		39.65	-66.16	32.70	-0.47

B. Velocity Profiles

Figure 5 shows the velocity profiles at 4 points along the upper surface of the plate. At $\frac{x}{c} = 0.031$ both models correctly predict the peak reverse flow velocity but the boundary layer profile is much steeper at the wall indicating a higher level of turbulence, indicating that they have not been able to model the relaminarisationn of the reversed boundary, although not visible in the figure, the velocity in the experimental curve is in the positive direction near the wall, indicating the presence of the secondary separation bubble. The K-ω model with no limiter shows a much greater reverse flow velocity as this section is closer to the centre of it's separation bubble, where reverse velocities are highest.

At $\frac{x}{c} = 0.5$ the two models with the Durbin limiter are still experiencing reversed meaning the are significantly off the experimental boundary layer profile, however they do match the freestream velocity fairly accurately. The SST model without the limiter has a profile much closer to the experimental data due to the proximity of the section to the reattachment point, however the profile shows a steeper near wall gradient followed by a nonlinear increase up to the freestream velocity which is underpredicted. The K-ω exhibits a very different profile as it has had a greater distance to develop and contains far more TKE, although inaccurate it does show the characteristic profile described in section A, with a thin layer of steep velocity gradient followed by a near linear rise to the freestream.

By the end of the plate, the differences in the experimental and simulated profiles become far clearer. The experimental profile has developed into the characteristic shape just described whilst the simulations show a similar profile to the one they had at the mid-chord, with a shallower non linear rise through the majority of the boundary layer. The non limited K-ω model matches the majority of the profile very well only deviating at the freestream.

a) $\frac{x}{c} = 0.031$

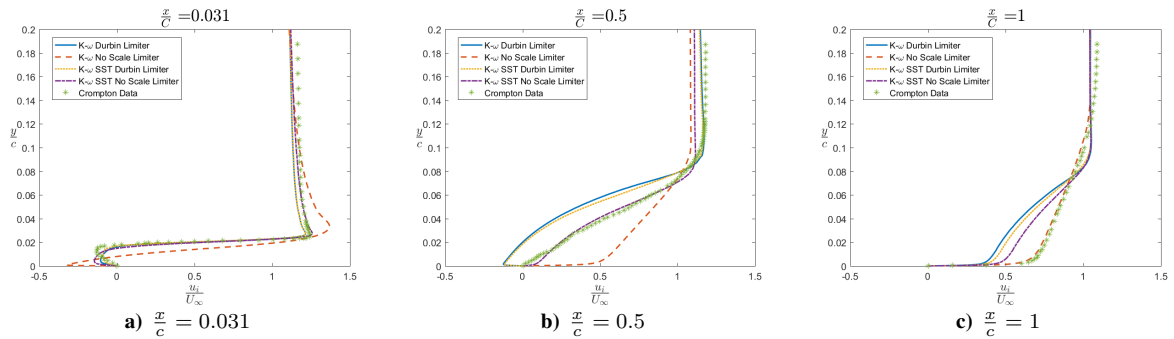**b) $\frac{x}{c} = 0.5$**

c) $\frac{x}{c} = 1$

Figure 5. Velocity Profiles

C. Turbulent Kinetic Energy Profiles

Figure 6 shows the velocity profiles at 4 points along the upper surface of the plate. These profiles help explain the differences identified in the velocity profiles above. $\frac{x}{c} = 0.031$ the experimental profile shows a brief inflection, indicating the more laminar boundary layer in the reversed flow region. Although the SST model with the Durbin limiter comes close, none of the simulated profiles have the same inflection indicating their fully turbulent nature. Only the non-limited K-ω model shows TKE values on a similar order of magnitude to experiment, this is because of the artificially high turbulence at the leading edge in this model.

At the mid-chord, the experimental values are closer to the simulations but still around twice as great, as well as this difference in magnitude, the experimental profile shows a higher concentration of TKE towards the wall, this fuels the development of the thin, steep gradient section of the velocity profile further down the chord. The non-limited K-ω profile has significantly reduced to a value below the other 3 models, the profiles of all 3 models have shifted upwards and more than in the experiment.

By the end of the plate the profiles have significantly changed, all 5 profiles are flatter but the distribution has shifted upwards far more in the non-limited K-ω model and experimental data, indicating a greater transfer of energy from the boundary layer to the freestream, this could explain the greater freestream velocity shown in the experimental data in figure 5c. The experimental profile shows a far greater concentration of TKE near the wall, indicating the injection of turbulence into the near wall region from above as described in A.
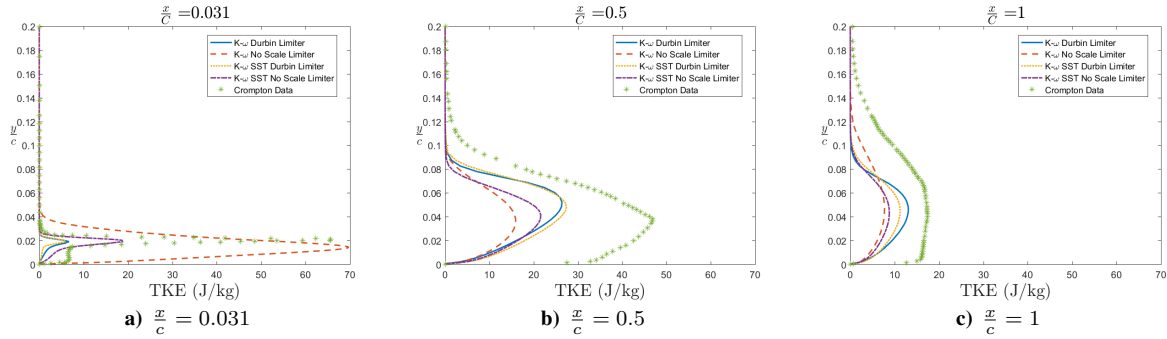

a) $\frac{x}{c} = 0.031$ **b)** $\frac{x}{c} = 0.5$ **c)** $\frac{x}{c} = 1$

Figure 6. Turbulent Kinetic Engergy Profiles

IV.   Conclusions

The complex case of flow past a sharp edged flat plate at incidence has been modelled using a variety of turbulence models, specifically K-ω and K-ω SST models both with and without a Durbin scale limiter and an anisotropic Reynolds Stress model. The results were compared to experimental results produced by Crompton [1]. None of the models were completely satisfactory, the Reynolds Stress models were unable predict the correct reattachment length and showed an anomolous flow feature and so were ignored in the discussed results. The other 4 models were able to reproduce the general shape of the separation. With the Durbin scale limiter activated, both the K-ω and K-ω SST models overpredicted the reattachment length by around 35% and subsequently displayed significantly different velocity profiles from the experimental data. The models with no scale limiter exhibited very different behaviour, the SST model was able to predict the reattachment length to with in 0.5%, whilst the standard K-ω model produced an unphysical peak in TKE (around $6\times$ greater than any other model) at the leading edge stagnation point. This in turn lead to the model predicting a reattachment length approximately one third of the experimental value. bar the non-limited K-ω model, all the models exhibit a flatter separation bubble with larger radii than in the experiment, thus experiencing less of a suction peak over the length of the bubble The cause in the difference in velocity profiles was discovered to be caused by the levels of TKE in the boundary layers produced by the models. The non limited K-ω model showed TKE values close to that of the experiment in close proximity to the leading edge but this quickly reduced to the point where it showed the lowest TKE values, this lead to the velocity profile quickly developing into the characteristic post-reattachment shape before remaining relatively constant over the remainder of the plate. The other 3 models showed some sign of the correct post reattachment profile but with a thinner high shear layer and a less linear rise to the freestream. They also showed less of a transfer of TKE to both the freestream and near wall region.

Collie, Rezende and Sampaio have all shown that Large Eddy Simulations are able to accurately predict the majority of the flow features over the plate including velocity profiles, turbulence distributions and the formation of the secondary separation bubble [2, 3, 4]. However this was not feasible with the resources available for this project. Collie states that the inherent instability in the real flat plate flow may be a cause of innaccuracy in the steady RANS results, it may therefore be useful to conduct and unsteady RANS simulation and investigate any increase in accuracy. A more suitable grid for capturing this flow would have been a boundary extruded O-type grid, unfortunately Star CCM+ does not have the ability to create these types of grid.

References

[1] Crompton, M. J. and Barrett, R. V., "Investigation of the separation bubble formed behind the sharp leading edge of a flat plate at incidence," *Proc. Inst. Mech. Eng. Part G J. Aerosp. Eng.*, Vol. 214, 2000, pp. 157–176.

[2] Collie, S., Gerritsen, M., and Jackson, P., "Performance of Two-Equation Turbulence Models for Flat Plate Flows With Leading Edge Bubbles," *J. Fluids Eng.*, Vol. 130, No. 2, 2008, pp. 021201.

[3] Rezende, A. L. T. and Nieckele, A. O., "Evaluation of TUrbulence Models to Predict the Edge Sparation Bubble over a thin Aerofoil," *COBEM*, ABCM, Gramado, RS, Brazil, 2009.

[4] Sampaio, L. E. B., Luiz T. Rezende, A., and Nieckele, A. O., "The challenging case of the turbulent flow around a thin plate wind deflector, and its numerical prediction by LES and RANS models," *J. Wind Eng. Ind. Aerodyn.*, Vol. 133, 2014, pp. 52–64.

[5] Peric, M. and Ferguson, S., "The advantage of polyhedral meshes," *CD-Adapco*, 2005.

[6] Ewing, P., "Best practices for," *Best Pract. Aerosp. Aerodyn.*, 2015.

[7] Andersson, B., Andersson, R., Håkansson, L., Mortensen, M., Sudiyo, R., and Van Wachem, B., "Turbulent-flow modelling," *Comput. Fluid Mech. Eng.*, chap. 4, Cambridge University Press, Cambridge, 2011, pp. 62–112.

[8] Park, C. H. and Park, S. O., "On the limiters of two-equation turbulence models," *Int. J. Comut. Fluid Dyn.*, Vol. 19, No. 1, 2005, pp. 79–86.